Environmental Science Advances

ROYAL SOCIETY OF CHEMISTRY

PAPER

View Article Online
View Journal | View Issue

Cite this: *Environ. Sci.: Adv.*, 2022, **1**, 110

A flexible copper sulfide composite membrane with tunable plasmonic resonance absorption for near-infrared light-driven seawater desalination†

Lu An, [a] Chengbin Wang,[a] Qunfeng Feng,[a] Zhenmin Xu, *[ab] Qiwei Tian, [a] Wei Chai, [c] Shiping Yang *[a] and Zhenfeng Bian *[a]

Near-infrared light driven devices for water evaporation are strictly limited by their inflexibility, high cost, complicated fabrication processes, and low energy-conversion efficiency. Here, a flexible copper sulfide composite membrane with tunable plasmonic resonance absorption for an efficient near-infrared light photothermal conversion is proposed. Both the uniformity of the morphology and the proportion of Cu^{+} in the flower-like copper sulfide (CuS) superstructure are easily controlled by adjusting the amount of polyvinylpyrrolidone (PVP), which effectively improves the absorption of the CuS superstructure in the near-infrared region. Furthermore, the flexible CuS/Matrimid composite membrane constructed by combining CuS and polyimide membranes exhibits highly flexible properties, strong NIR absorption, fast heating (10 s), and good thermal stability. A highly efficient photothermal conversion is achieved by near-infrared light-driven water evaporation. Under 808 nm light irradiation, the water evaporation conversion efficiency is *ca.* 80% and has excellent evaporation stability. The flexible CuS/Matrimid composite membrane developed in this study could have promising practical applications in near-infrared light-driven devices for seawater desalination.

Received 10th December 2021
Accepted 26th January 2022

DOI: 10.1039/d1va00043h

rsc.li/esadvances

Environmental significance

The seawater desalination driven by solar steam has emerged as one of the most promising ways to address this problem, due to its low energy input, high evaporation efficiency, and easy operation. NIR photothermal conversion materials, which can convert most of the NIR light energy into heat energy, can greatly improve the efficiency of NIR light utilization. Copper sulfide, as an easy to fabricate doped semiconductor, shows excellent photostability, adjustable NIR absorption, and outstanding energy transfer efficiency. A NIR light-driven flexible hot plate by incorporating doped semiconductors with a flexible polymer membrane realizes the potential utility of the NIR light and doped semiconductors in seawater desalination.

1 Introduction

Water is the source of human life and the foundation of all things. It is because of moist water that the earth appears to be full of vitality, thriving. However, the rapid development of industrialization and modernization has led to the gradual reduction of available clean water resources.[1,2] Seawater desalination driven by solar steam emerges as one of the most promising ways to address this problem, due to its low energy input, high evaporation efficiency, and easy operation.[3] Generally, photothermal materials floating on the water surface or adhered to the container wall absorb sunlight, so as to carry out heat conversion and transfer, and generate water vapor through interface heating. However, the water evaporation efficiency was still inhibited by the high cost, poor stability, complicated fabrication processes, and low efficiencies of photothermal materials for solar light absorption, especially broadband near-infrared (NIR, 780–2526 nm) light.[4,5] Therefore, it is imperative that novel NIR-driven materials or devices are devised, which have a high NIR utilization efficiency, so as to broaden the possible scope of application.

NIR photothermal conversion materials, which can convert most of the NIR light energy into heat energy, can greatly improve the efficiency of NIR light utilization. Doped semiconductors, noble metal nanostructures, organic polymers and carbon materials are four typical kinds of NIR photothermal conversion materials that are widely used in the field of NIR light conversion.[6–9] In order to effectively use NIR light, several

[a]*The Education Ministry Key Laboratory of Resource Chemistry, International Joint Laboratory of Resource Chemistry, Shanghai Normal University, Shanghai 200234, China. E-mail: zhenminxufy@163.com; shipingy@shnu.edu.cn; bianzhenfeng@shnu.edu.cn*

[b]*School of Chemical and Environmental Engineering, Shanghai Institute of Technology, Shanghai 201418, China*

[c]*Department of Chemical Engineering, Zaozhuang Vocational College, Zaozhuang, Shandong, 277800, China*

† Electronic supplementary information (ESI) available. See DOI: 10.1039/d1va00043h

devices have been built recently based on NIR photothermal conversion materials. For example, Sun *et al.* constructed NIR light-induced shape memory polymers and silver nanoparticles for healing mechanical damage;[10,11] a carbon nanotube composite[12] and organic polymer[13,14] were used as NIR light-driven photothermal-electrical and photo-magneto-thermo-electric devices by Wang *et al.* and Kim *et al.*, respectively. Doped semiconductors, mainly including copper chalcogenide compounds ($Cu_{2-x}E$, E = S, Se, Te)[15] and transition metal oxides (WO_{3-x}, MoO_{3-x}, Mn_xO_y, *etc.*),[16,17] are a class of defect semiconductors with a local surface plasmon resonance (LSPR) effect. Compared with noble metal nanostructures, organic polymers, and carbon materials, doped semiconductors feature the advantages of low cost and stability.[18] Song *et al.* developed Cs_xWO_3 nanoparticles to enhance the upconversion luminescence of monolayer upconversion nanoparticles as a high performance narrowband NIR photodetector, demonstrating the potential advantages of doped semiconductors.[19] Hence, it is meaningful to further explore NIR light-driven devices constructed from doped semiconductors, such as a NIR light-driven flexible hot plate by incorporating doped semiconductors with a flexible polymer membrane, to realize the potential utility of NIR light and doped semiconductors in seawater desalination.

Copper sulfide, one of the most easily prepared doped semiconductors, shows excellent photostability, adjustable NIR absorption, and outstanding energy transfer efficiency,[15] and has been broadly applied to solar cells, catalysts, pollutant degradation, supercapacitors, and biomedicine.[20–23] Matrimid® 5218, a thermoplastic polyimide based on 5(6)-amino-1-(4′-aminophenyl)-1,3-trimethylindane, is soluble in a variety of common solvents and will leave a strong, durable, and high temperature-resistant flexible coating.[24,25] More importantly, it is easy to cut into any shape and can be placed in any location. Thus, once inorganic materials are introduced into the polymer matrix, a combined effect of its polymeric and inorganic components' properties is thought to ensue. Therefore, here we propose a NIR light-driven flexible hot plate based on the introduction of copper sulfide into Matrimid® 5218, whereby copper sulfide can absorb NIR light and Matrimid® 5218 provides flexibility and endows the polymer matrix with high temperature resistance. This integrated device may show potential applications in seawater desalination with the synergy of the two components.

The main challenge for this proof-of-concept experiment is to fabricate a uniform copper sulfide-Matrimid® 5218 flexible membrane with strong NIR absorption. To do this, we relied on several steps. Firstly, *N*-methyl-2-pyrrolidinone (NMP), which is normally used to dissolve Matrimid® 5218, was used as a solvent to prepare the copper sulfide nanocrystals. Thus, both the obtained copper sulfide nanocrystals and Matrimid® 5218 are soluble in the same solvent, uniformly. After the evaporation of NMP, a strong, durable, uniform, and flexible copper sulfide-Matrimid® 5218 membrane was obtained. Secondly, to attain adequate absorption of NIR light, the doping state and morphology of copper sulfide nanocrystals were tuned, accordingly, by simply controlling the PVP content. Finally, once irradiated with NIR light, the copper sulfide-Matrimid® 5218 membrane's temperature rises rapidly, enabling its use as a NIR light-driven flexible hot plate. The applications of this devised NIR light-driven flexible hot plate in photothermal evaporation water were also explored. Due to its impressive photothermal effect and flexible cutting advantages, this novel hot plate can be placed on either the outer or the inner surface of a given device, to prevent salt precipitation from accumulating on the surface, thereby enhancing the overall evaporation efficiency.

2 Experimental

PVP (M_w = 29 000) was purchased from Sigma Aldrich. Copper(II) sulfate pentahydrate ($CuSO_4 \cdot 5H_2O$), *N*-methyl-2-pyrrolidinone (NMP), sulfur, and polyimide were all purchased from Sinopharm Chemical Reagent Co., Ltd.

2.1 Preparation of the flower-like CuS nanostructure

First, 0.5 g of PVP was dissolved in 15 mL of NMP, and then 0.5 mM (0.125 g) $CuSO_4 \cdot 5H_2O$ was added to the PVP solution under magnetic stirring. This stirring was continued until a bright green transparent solution was obtained, and then 1 mM sulfur powder (0.032 g) was added to the mixed solution. After 10 min of stirring, the above solution was transferred into a 25 mL Teflon autoclave for the reaction at 180 °C for 4 h. The black-green CuS was centrifuged and washed twice with NMP, and dissolved in 1 mL of NMP for its later use.

2.2 Preparation and characterization of the CuS/Matrimid composite membrane

Polyimide (0.2 g) was mixed with 1 mL of CuS in differing amounts (*i.e.*, 1, 2, 5, and 10 mg mL^{-1}). After undergoing thorough mixing, an appropriate amount of a given sample was added dropwise onto a glass pane and we manually scraped the 500 μm surface with a membrane coater. Then it was quickly placed in a vacuum-drying oven and dried with a gradient temperature series: 80 °C for 12 h, 140 °C for 1 h, and 200 °C for 1 h.

For absorption measurements, a blank PI membrane without CuS served as the baseline. The absorbance of the CuS/Matrimid composite membrane generated with different amounts of CuS was measured accordingly.

For testing its photothermal properties, the blank membrane and CuS/Matrimid composite membrane were cut into small disks (2 cm diameter). An 808 nm laser (1 W cm^{-2}) was used to irradiate the top of each membrane, whose temperature change was recorded with a thermal imaging device.

2.3 Characterization

The structure of the CuS nanostructure was confirmed by X-ray diffraction (XRD, Rigaku DMAX2000), and its morphology was quantitatively examined by SEM (JEOL JEM-6460A) and TEM (JEOL TEM-2100). The electronic state of Cu in the flower-like CuS was determined by X-ray photoelectron spectroscopy (ESCALAB 250Xi), and the absorbance of the CuS nanostructure and CuS/Matrimid composite membrane was determined by UV-Vis-NIR (Beckman Coulter DU730) and UV-Vis diffuse

reflectance spectroscopy (Shimadzu UV-2450). The heating effect was tracked by using a FLIR A300 thermal imaging device.

2.4 Vapor generation by the CuS/Matrimid composite membrane hot plate

The saltwater sample (26.5 g L^{-1} NaCl, 0.2 g L^{-1} $NaHCO_3$, 0.28 g L^{-1} NaBr, 24 g L^{-1} $MgCl_2$, 3.3 g L^{-1} $MgSO_4$, 0.73 g L^{-1} KCl, and 1.1 g L^{-1} $CaCl_2$) and sewage sample (3.5 wt% NaCl, 10 ppm *p*-chlorophenol) were respectively prepared according to previous reports.[4,26] The seawater was collected from the East China Sea, in Fengxian (Shanghai).

The CuS/Matrimid composite membrane was cut into a square (1 cm × 1 cm) and this was stuck to the outside wall of a cuvette filled with water. The composite membrane was irradiated with an 808 nm laser (2 W cm^{-2}) for 900 s, and water temperature was recorded with a thermal imaging device. Two key parameters, the water evaporation rate (ν) and water evaporation efficiency (η), were calculated using eqn (1) and (2), respectively.

$$\nu = \frac{m_{\text{loss}}}{\pi\left(\frac{D}{2}\right)^2 t} \quad (1)$$

where m_{loss} is the mass of evaporated water, D represents the diameter (0.5 mm) of the light spot, and t is the evaporation time.[27]

$$\eta = \frac{H_e \times \nu}{Q_s} \quad (2)$$

where H_e denotes the total enthalpy of the liquid water-to-vapor phase transition (J g^{-1}), ν is the water evaporation rate, and Q_s is the light density of solar illumination.[28]

For the solar water desalination test, the CuS/Matrimid composite membrane was pasted on the inside of a 100 mL aluminum cup to better absorb solar energy. The aluminum cup

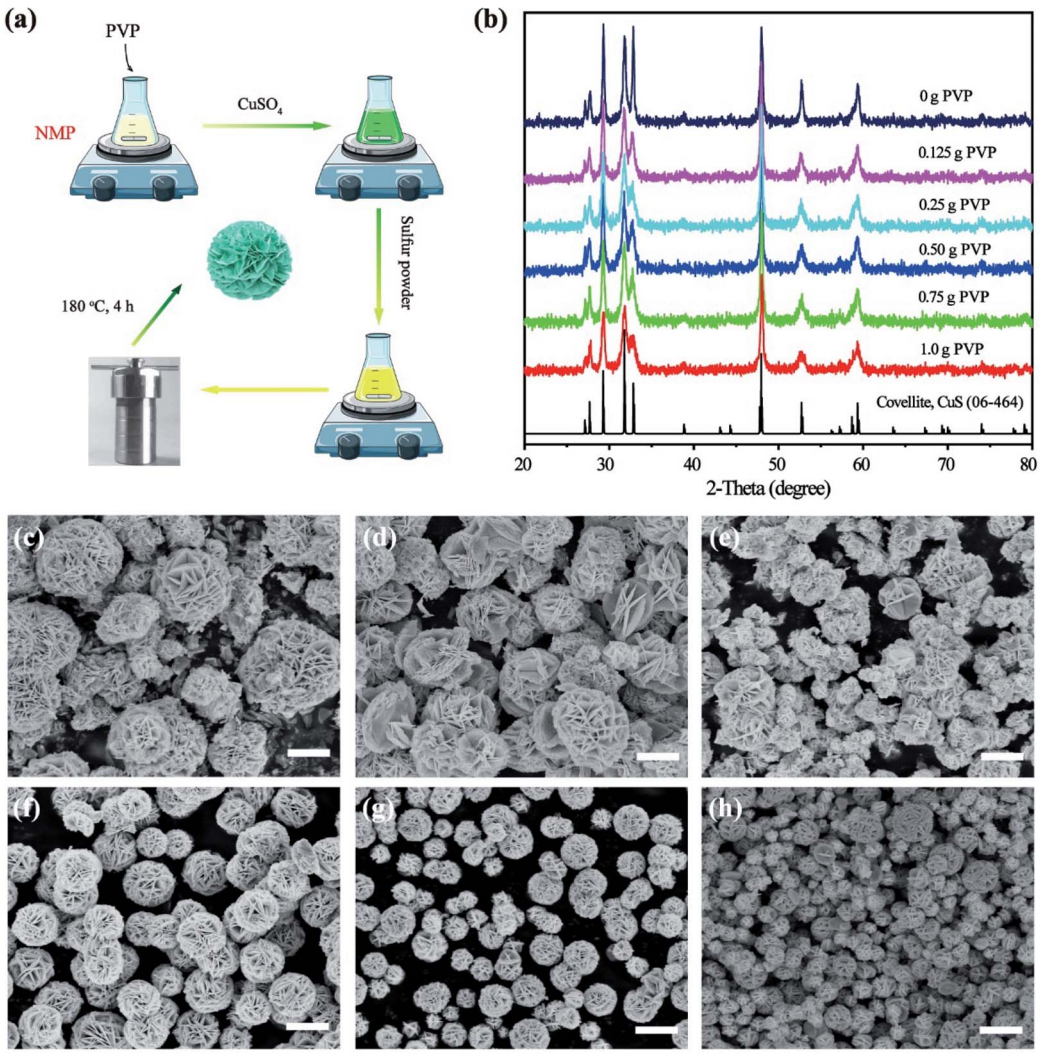

Fig. 1 (a) Schematic illustration of the preparation of superstructure CuS nanoparticles. (b) X-ray diffraction (XRD) results of CuS without and with different amounts of PVP. (c–h) SEM images of flower-like CuS without and with different amounts of PVP (0, 0.125, 0.25, 0.5, 0.75 and 1 g, respectively). Scale bar = 2 μm.

was then filled with seawater and irradiated with a xenon lamp at a power density of 1 W cm^{-2}. Both photothermal imaging and water temperature were recorded with a thermal imaging device (FLIR A310).

3 Results and discussion

3.1 Tuning the NIR absorption of the CuS nanocrystals

To obtain copper sulfide nanocrystals with high photothermal conversion efficiency, some rational designs have been adopted to enhance their absorption of NIR light, for example, by tuning the structure, copper deficiency, and hybrid composite. Nearly all of these methods are used in hydrothermal or thermal decomposition processes. But in order to prepare a uniform copper sulfide-Matrimid® 5218 flexible membrane, a solvothermal method must be implemented that is able to synthesize the copper sulfide by using NMP as the solvent. In this study, the copper sulfide was synthesized by a solvothermal method that uses PVP as the surfactant and NMP as the solvent (Fig. 1a). The effects of PVP content on the crystal phase, shape, copper valence and NIR absorption of the copper sulfide were analyzed.

Previous reports have demonstrated that the crystal phase is critical for tuning the localized surface plasmon resonance (LSPR) absorption for copper sulfide.[29,30] Thus, the effect of PVP content on the crystal phase was first investigated. The copper sulfide was prepared solvothermally by adding sulfur and $CuSO_4$ into NMP with differing amounts of PVP (0–1 g). The structural changes of the obtained copper sulfide samples were then investigated by studying the X-ray diffraction (XRD) patterns (Fig. 1b). The main diffraction peaks situated at the 2θ angles of 29.28, 31.81, 32.95, 47.93, 52.71, and 59.34 of the copper sulfide prepared without PVP (*i.e.*, 0 g added) agreed well with the (102), (103), (006), (110), (108), and (116) lattice planes of covellite CuS (JACPDS card no. 06-464). No characteristic peak can be indexed to any other phase of copper sulfide, except covellite CuS. When PVP was added in amounts of 0.125 to 1 g, evidently the peak patterns maintained the same structure as that of covellite CuS, while the intensity of characteristic peaks at the 2θ angle of 32.95 decreased a little. This change in peak intensity may be attributed to the growth of the (006) lattice plane being inhibited by the strong coordination of PVP and Cu^{2+}. The XRD patterns for copper sulfide obtained in the absence and presence of PVP suggest that PVP shows no apparent effects on the crystal phase of copper sulfide.

Next, the morphology of the copper sulfide obtained with and without PVP was observed by scanning electron microscopy (SEM). The CuS material prepared without PVP is composed of a large-sized flower-like superstructure and irregular nanoparticles (Fig. 1c), while a more uniform flower-like superstructure smaller in size was obtained when PVP was introduced (Fig. 1d–h). PVP is competent to stabilize the CuS superstructure. In the chemical sintering process, the small particles will form compact solids due to the coalescence and Ostwald ripening behaviors triggered by the detachment of PVP.[31] With more PVP added, the growth of the CuS superstructure can be reliably controlled, and the flower-like superstructures of CuS appear uniform (Fig. S1†), which ought to improve the photon reflection capacity and the NIR absorption and further enhance the photothermal conversion effect. In addition, the size of the CuS superstructure can also be tuned by changing the PVP content. As the SEM images show, the size of the prepared CuS superstructure decreased 10-fold, from 10 to 1 μm, when the PVP content is increased from 0 to 1 g; this indicated that the higher the PVP content used, the smaller is the size of the CuS superstructure. These results demonstrated that the uniformity and size of the superstructure, which are beneficial to promote the photothermal conversion effect, are governed by the PVP content.

Given that the electronic state of Cu is related to the hole density of the nanomaterials, which is crucial for NIR absorption, XPS measurements were conducted to confirm the electronic state of Cu in the prepared CuS nanostructures. The Cu 2p peaks of these CuS featured the typical asymmetric tail of covellite.[32] Without PVP present, the binding energy intensity values of Cu $2p_{3/2}$ and Cu $2p_{1/2}$ were slightly left-shifted to 932.24 and 952.12 eV, with weak satellite peaks at 942.07 observed, indicating the presence of typical Cu^{2+} but little Cu^{+} in the obtained CuS nanostructures.[33–35] As more PVP was used, the two binding energy intensity values of Cu $2p_{3/2}$ and Cu $2p_{1/2}$ were increasingly right-shifted and their satellite peaks gradually decreased, suggesting a greater proportion of Cu^{+} in the CuS nanostructures (Fig. 2a). Moreover, the S 2p band of these CuS also corresponded to the typical "three peaks" of covellite, and the disulfides eventually disappeared as the amount of PVP increased, thus indicating a gradual shift to chalcocite (Fig. S2†). To clarify the ratio of Cu^{2+} to Cu^{+} in the CuS nanostructures, their Cu 2p bands were adequately fitted to four curve-fitting bands. Using the area of the four curve-fitting bands, the ratio of Cu^{2+} to Cu^{+} was calculated accordingly, yielding values of 0.71, 0.34, 0.32, 0.30, 0.27, and 0.28 (Fig. 2b and c). The results suggest that the ratio of Cu^{+} in the CuS nanostructures increases as the amount of PVP increases until it's reduced to saturation, which can be ascribed to the effect of precursor reducibility by PVP.[36,37]

The optical properties of CuS prepared by introducing various amounts of PVP were examined by Vis-NIR spectroscopy. To fairly compare the absorption intensity of these differently prepared CuS samples, their absorption at 650 nm was assigned the same value. With more PVP added, the normalized absorption intensity of the obtained CuS nanostructure in the NIR region (700–1000 nm) clearly increased (Fig. 2d). Moreover, absorption at 808 nm is linearly enhanced with increasing PVP content, until it reaches saturation when 0.75 g of PVP is added (Fig. 2e). The NIR absorption of CuS is the LSPR absorption of electrons and holes, which is like the LSPR absorption of electrons in the noble metal. The hole arises from the copper vacancy in the CuS nanoparticles, such that CuS nanoparticles with a higher hole density will exhibit stronger NIR absorption.[38,39] The copper vacancy can be tuned by modulating the proportion of Cu^{+} in the CuS nanostructure, yet the Cu^{+} in the CuS nanostructure can be controlled by the applied amount of PVP in the synthesized system. In addition, the superstructure facilitates the NIR absorption of CuS

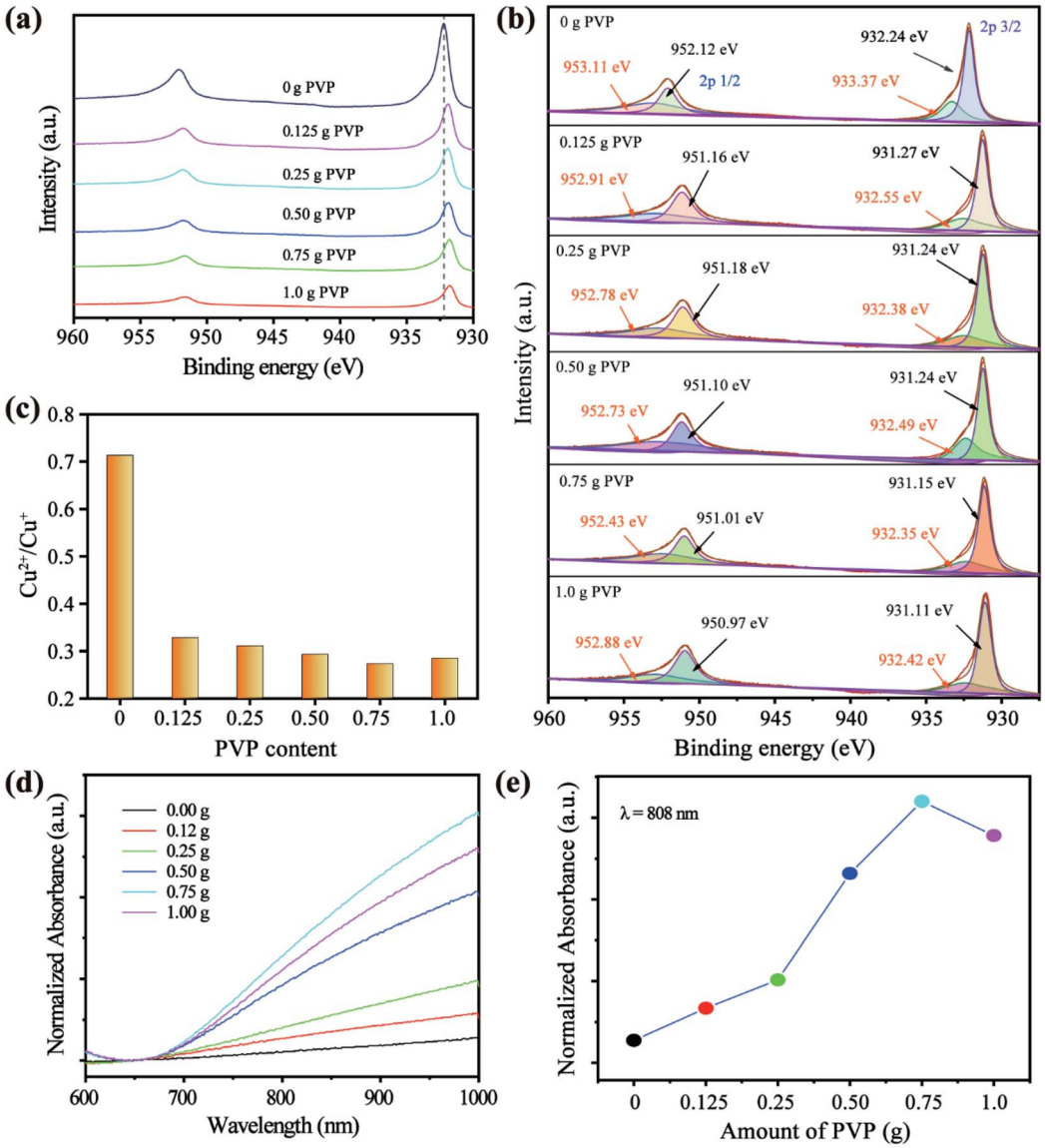

Fig. 2 (a) X-ray photoelectron spectroscopy (XPS) of Cu 2p of the obtained flower-like CuS nanostructures, without and with different amounts of PVP. (b) High-resolution spectra of Cu 2p of CuS nanostructures. (c) Ratio of Cu^{2+} to Cu^{+} according to the fitting curves in (b). (d and e) Vis-NIR spectrum of the flower-like CuS without and with different amounts of PVP (d), and (e) the corresponding absorbance value at 808 nm.

nanoparticles, likely because photo-absorption can be augmented by the faceted end planes of well-shaped crystals that serve as good light-cavity mirrors.[40,41] This inference is also corroborated by our finding of the NIR absorption of the CuS superstructure decreasing after undergoing ball milling (Fig. S3†). Therefore, the strong LSPR absorption of CuS in the NIR region can be simply tuned by the amount of PVP used in the synthesis system.

3.2 Preparation and characterization of the flexible hot plate based on the CuS/Matrimid composite membrane

Materials with flexibility, ease of cutting, and ease of construction are now receiving extensive attention from researchers. To broaden the application scope of the CuS nanostructure with strong NIR absorption, it would be prudent to develop a CuS flexible membrane with excellent photothermal properties. Matrimid® 5218 is a widely used polymer matrix for various inorganic nanoparticles in microelectronics and the gas separation industry. More importantly, the Matrimid® 5218 membrane has good heat-resistance. Here, we developed a flexible hot plate by incorporating the CuS nanostructure into Matrimid® 5218 uniformly. The CuS nanostructure was prepared in NMP and it can be dispersed in NMP very well, while the NMP performs well as a solvent for the Matrimid® 5218 polymer. Thus, a uniformly dispersed liquid of the CuS nanostructure and Matrimid® 5218 was easily obtained when they were added to NMP with ultrasonic dispersion. Following this step, the CuS/Matrimid membrane was prepared by applying a scrape coating/drying technique (Fig. 3a). The doped

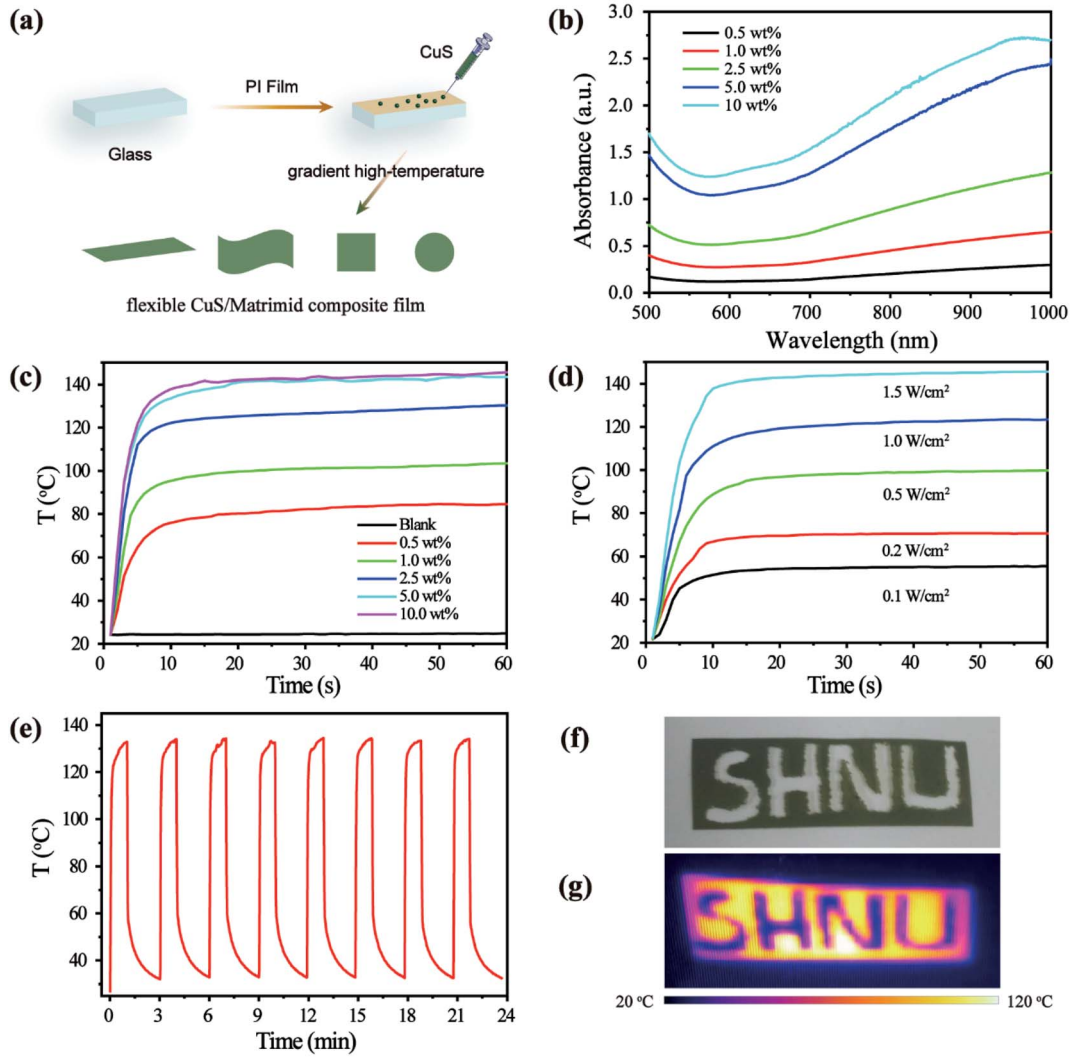

Fig. 3 (a) Scheme for the preparation of the CuS/Matrimid composite membrane. (b) Absorption spectrum of the CuS/Matrimid composite membrane with different doped amounts of CuS. (c) Profile of enhanced temperature *vs.* irradiation time of the 808 nm laser (light density = 1 W cm^{-2}) for the CuS/Matrimid composite membrane with different doped amounts of CuS and (d) with a different light density for the membrane (2.5 wt%). (e) Photostability of the CuS/Matrimid composite membrane with 2.5 wt% CuS. (f and g) Photograph (f) and corresponding NIR thermal imaging (g) of the obtained CuS/Matrimid composite membrane.

amount of the CuS nanostructure in the membrane is controlled by the added weight of CuS and Matrimid® 5218. The structure of the dispersed CuS in the prepared CuS/Matrimid membrane was verified by XRD (Fig. S4†). The strong diffraction peaks located at the 2θ angles of 29.28, 31.81, 47.94, and 53.02 respectively correspond to the (102), (103), (110), and (108) lattice planes of standard hexagonal CuS, which proves that the phase structure of CuS in the membrane is stable and does not change.

The absorption performance of the fabricated membranes with increased levels of CuS doping (0.5 wt%, 1.0 wt%, 2.5 wt%, 5.0 wt%, and 10 wt%) was evaluated from their Vis-NIR spectra (Fig. 3b). The absorption values rose considerably by increasing the CuS doping from 0.5 wt% to 10 wt% for the CuS/Matrimid composite membrane. Its good absorption properties in the NIR region will confer an excellent photothermal performance. We then tested its photothermal performance by recording the temperature change under 808 nm laser (1 W cm^{-2}) irradiation for 60 s (Fig. 3c). Compared with the blank Matrimid membrane, the CuS-doped Matrimid membrane exhibited outstanding photothermal performance, in which the temperature is capable of rising from 84.5 °C to 145.5 °C when the doped CuS content is increased from 0.5 wt% to 10 wt%. Furthermore, the temperature increase of the CuS/Matrimid composite membrane is particularly fast under the laser irradiation, attaining its maximum in just 10 s. After that, the temperature can maintain its maximal value without undergoing significant change, which is attributable to the generated heat from the CuS/Matrimid composite membrane under the laser irradiation being equal to the heat diffused into air. These results suggest that the CuS/Matrimid composite membrane has the property of fast heating under laser irradiation.

Next, the relevance of light density for the photothermal properties of the CuS/Matrimid composite membrane was

investigated (Fig. 3d). For the CuS/Matrimid composite membrane with 2.5 wt% CuS, the maximum temperature reachable by the CuS/Matrimid composite membrane is 55 °C to 145 °C under irradiation of a laser with a light density from 0.1 to 1.5 W cm^2; this implies that light density exerts important effects. Thermal stability is a key parameter that determines whether the CuS/Matrimid composite membrane can be used as a hot plate. To evaluate it, the photothermal circle test was used. After 8 'on/off' cycles of the laser—each cycle consisting of a laser on time of 1.5 min and a laser off time of 1.5 min—the CuS/Matrimid composite membrane still exhibited similar photothermal properties, indicating very good thermal stability (Fig. 3e), which can be attributed to its structural stability after laser irradiation (Fig. S5†). Moreover, the prepared CuS/Matrimid composite membrane still possessed its highly flexible properties on par with those of the Matrimid® 5218 membrane without doping the CuS nanostructure, as demonstrated by the photographed Matrimid® 5218 membrane before (upper panel) and after (lower panel) doping the CuS nanostructure (Fig. S6†). In addition, the as-prepared membrane could be carved into many different shapes (Fig. 3f), without any influence on its impressive photothermal performance (Fig. 3g), endowing it with more potential for realistic applications. The excellent performance of the CuS/Matrimid composite membrane, characterized by its highly flexible properties, strong NIR absorption, fast heating, good thermal stability and easy cutting, makes it a promising candidate for use in a NIR light-driven hot plate.

3.3 NIR light-driven photothermal evaporation water based on the flexible CuS/Matrimid composite membrane hot plate

Due to the high photothermal performance and feasibility of the as-prepared CuS/Matrimid composite membrane, we reckon it can potentially pave the way for designing various devices that can be simply driven by NIR light. The efficient conversion of energy for vapor generation holds great promise for both desalination and water purification goals. Thus, we introduced the as-prepared CuS composite membrane for

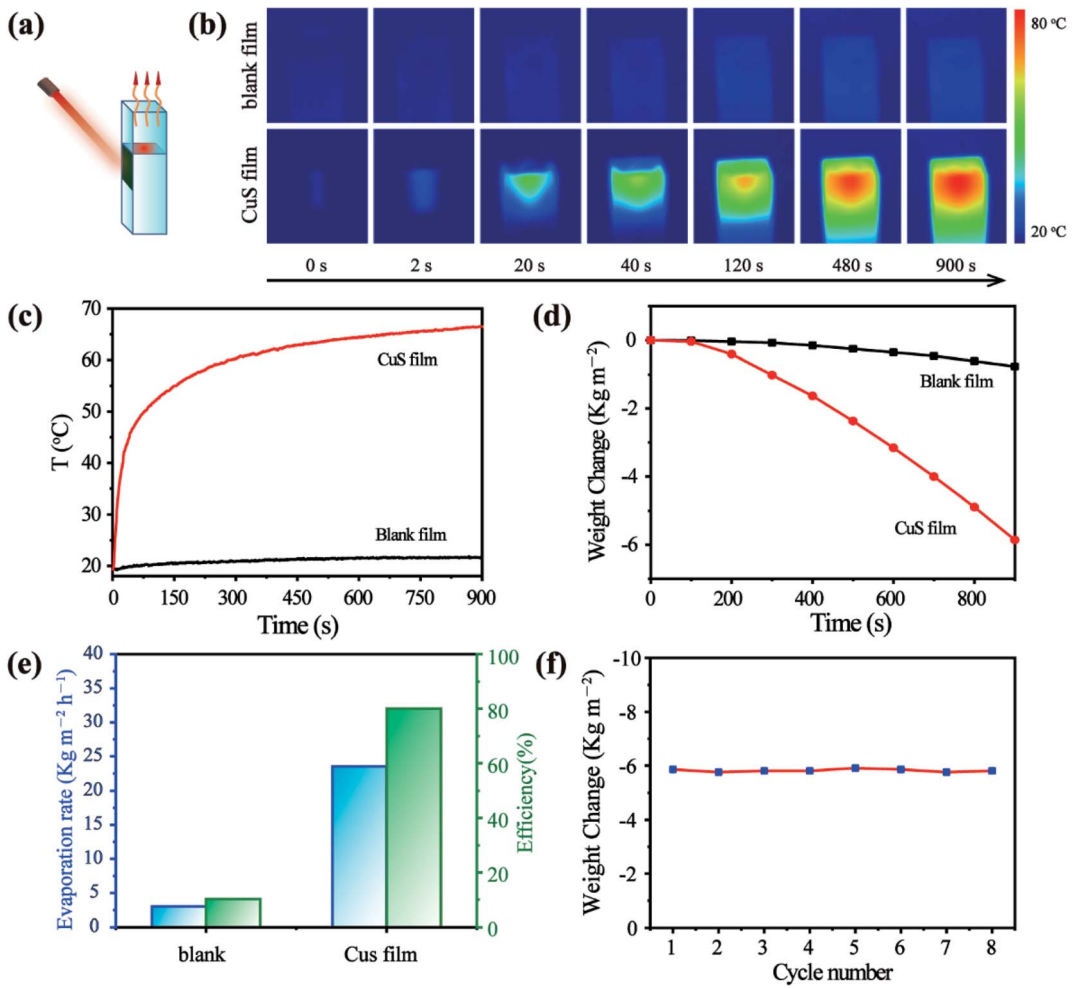

Fig. 4 (a) Scheme of the NIR light-driven photothermal evaporation water device. (b and c) Photothermal images (b) and the corresponding heating curve (c) of the blank membrane and CuS/Matrimid composite membrane (1.0 wt%) irradiated with an 808 nm laser for various durations of time. (d) Mass loss curve of water in the presence or absence of CuS. (e) Water evaporation rate (left, blue histograms) and evaporation efficiency (right, green histograms) of the blank membrane and CuS/Matrimid composite membrane, respectively. (f) Vapor generation cycle of the CuS/Matrimid composite membrane under 808 nm laser irradiation.

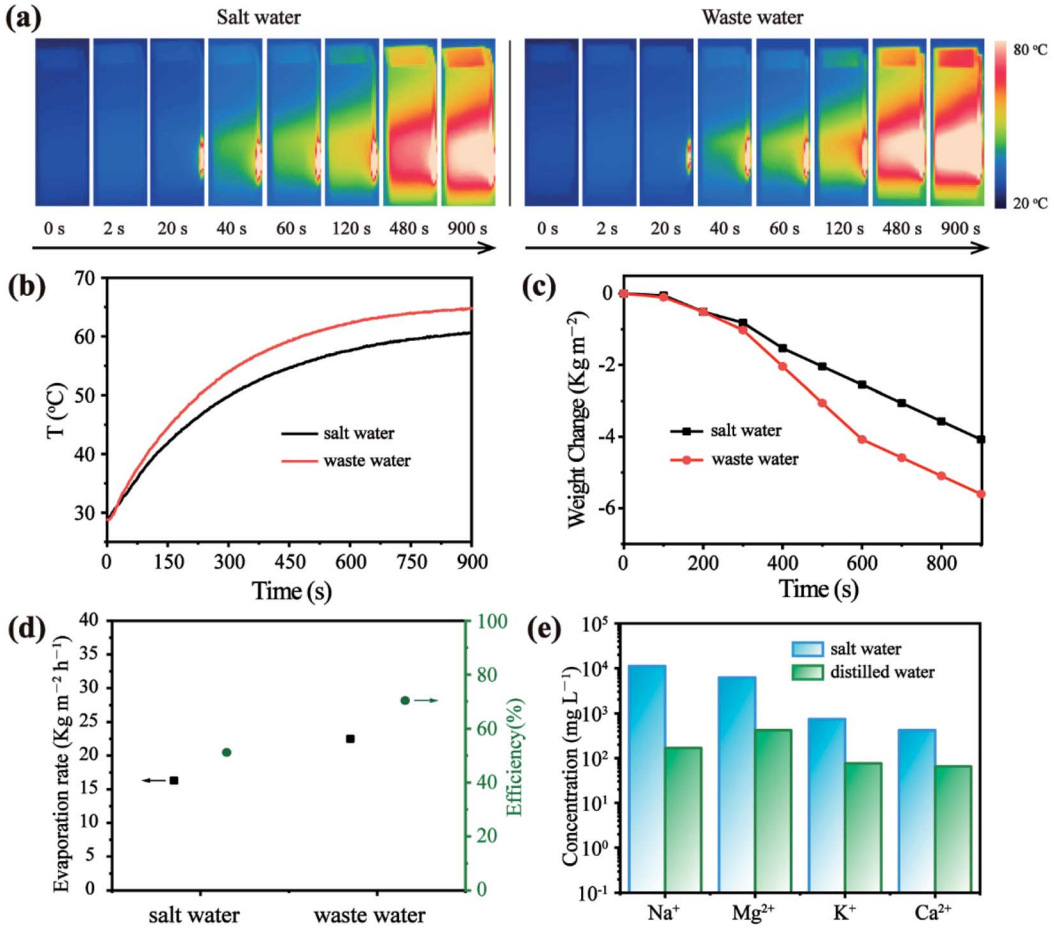

Fig. 5 (a) Photothermal images of salt water and wastewater covered by the CuS/Matrimid composite membrane and irradiated with an 808 nm laser. (b) The corresponding heating curve of (a). (c) Changes in the weight of tracked salt water and wastewater covered by the CuS/Matrimid composite membrane under laser irradiation. (d) Water evaporation rate and evaporation efficiency of salt water and wastewater, calculated according to (c). (e) Changed ions' concentration of salt water after desalination.

highly efficient vapor generation by heat localization at the evaporation surface (Fig. 4a). Evidently, with the CuS membrane present, the temperature rose rapidly under continuous laser irradiation and remained stable for the entire 900 s duration. In stark contrast, the temperature in the blank panel showed only a slight difference after its irradiation (Fig. 4b and c). Moreover, the cumulative weight loss was positively correlated with the irradiation time (Fig. 4d). Under 808 nm irradiation, the weight loss over the 900 s period was 5.86 kg m^{-2}, and the steady-state evaporation rate was calculated to be 23.4 kg m^{-2} h^{-1}. This is much higher than the evaporation rate of water in the absence of CuS, which was 3.06 kg m^{-2} h^{-1}. Hence, the photothermal evaporation conversion efficiency of the CuS/Matrimid composite membrane ($\approx$80%) is nearly 8 times higher than that of the blank membrane (Fig. 4e). Crucially, the steady-state evaporation rate and cumulative weight loss did not change significantly over eight cycles of reuse (Fig. 4f). This suggests that the CuS/Matrimid composite membrane is highly stable and can be reused multiple times without a pronounced decrease in its evaporation capacity.

The NIR light-driven photothermal evaporation of water was also investigated in stimulated saltwater and wastewater. As expected, under continuous irradiation of the laser, both salt water and wastewater covered by the CuS/Matrimid composite membrane incurred a rapid heating effect (Fig. 5a). Due to the relatively complex nature and high concentration of ions in salt water, its temperature rise is affected to some extent (Fig. 5b). Accordingly, the weight change of salt water after evaporation is not as great as that of wastewater or pure water (Fig. 5c). Nonetheless, much water was still evaporated within 15 min, and the evaporation rate and efficiency of salt water and wastewater are still good (Fig. 5d). More importantly, after water evaporation, the concentration of ions in the collected distilled water had decreased substantially (Fig. 5e). In addition, the evaporation of the composite membrane is relatively stable (Fig. S7†). Solar seawater evaporation and desalination tests showed similar heating and desalination effects, thus indicating that the CuS/Matrimid composite membrane may be useful for light-driven photothermal evaporation of water (Fig. S8†). Overall, because of its strong NIR absorption, high photothermal conversion, flexible cutting and localization, the

CuS/Matrimid composite membrane shows great photothermal efficiency, which we anticipate will be applied in actual water evaporation and seawater desalination projects.

4 Conclusion

In summary, a kind of flower-like, self-doped CuS superstructure with tunable plasmonic resonance absorption and photothermal effects was designed, for which PVP was the surfactant and NMP is the solvent. The results show that with a greater amount of added PVP, there is an increased degree of Cu^{2+} reduction, generating more copper defects that enhance the absorption ability of the CuS superstructure in the near infrared region, until Cu^{2+} is no longer reduced. Furthermore, CuS membranes featuring high-temperature resistance and good flexibility were prepared by combining CuS with polyimide membranes *via* coating and gradient high-temperature curing. Photothermal performance testing shows that the temperature of the CuS/Matrimid composite membrane can rise to more than 100 °C within just a few seconds under the irradiation of an 808 nm laser, suggesting that it functions as a robust photothermal conversion membrane. The responsive properties of the CuS/Matrimid composite membrane to vapor evaporation driven by NIR light were explored. Compared with a blank membrane, the composite membrane evinced a heating effect and better evaporation efficiency, both in stimulated saltwater and sewage. This proves that the CuS/Matrimid composite membrane has promising application prospects. This work provides the possibility for further development of an NIR light-driven flexible and tunable absorption semiconductor, which we anticipate will broaden the further application of this kind of device.

Author contributions

L. A. conceived the original idea. Z. X., S. Y. and Z. B. supervised the project. L. A. and Q. T. designed and performed the experiments. L. A., C. W., Q. F. and W. C. performed the photocatalytic performance analysis. L. A. and Q. T. wrote the draft manuscript. Z. X., S. Y. and Z. B. revised the manuscript.

Conflicts of interest

The authors declare no competing financial interest.

Acknowledgements

This work was supported by the National Key Research and Development Program of China (2020YFA0211004), National Natural Science Foundation of China (22007066, 22176128, 21876114, and 21906105), sponsored by the Program of Shanghai Academic Research Leader (21XD1422800) and Shanghai Sailing Program (19YF1436200). Shanghai Government (19DZ1205102, 19160712900), Chinese Education Ministry Key Laboratory and International Joint Laboratory on Resource Chemistry, Shanghai Engineering Research Center of Green Energy Chemical Engineering (18DZ2254200), and Shanghai Eastern Scholar Program, "111 Innovation and Talent Recruitment Base on Photochemical and Energy Materials" (No. D18020), Shanghai Engineering Research Center of Green Energy Chemical Engineering (18DZ2254200) and Shanghai Frontiers Science Center of Biomimetic Catalysis.

References

1 X. Hao, G. Chen and Z. Yuan, Water in China, *Water Res.*, 2020, **169**, 115256.
2 J. Guo, D. Deng, J. Qiu, J. Shen, L. Wang, S. Wei, X. Zhang, Q. Zhou, H. Yu and W. Shi, Biodirected Identification of Untargeted Toxicants in Industrial Wastewater Guides the Upgrading of Water Treatments, *Environ. Sci. Technol. Lett.*, 2021, **8**, 474–481.
3 R. Chen, T. Zhang, J. Kim, H. Peng, M. Ye and C.-H. Huang, Interfacial Solar Distillation for Freshwater Production: Fate of Volatile and Semivolatile Organic Contaminants, *Environ. Sci. Technol.*, 2021, **55**, 6248–6256.
4 J. Deng, S. Xiao, B. Wang, Q. Li, G. Li, D. Zhang and H. Li, Self-Suspended Photothermal Microreactor for Water Desalination and Integrated Volatile Organic Compound Removal, *ACS Appl. Mater. Interfaces*, 2020, **12**, 51537–51545.
5 L. Yang, Y. Xiang, F. Jia, L. Xia, C. Gao, X. Wu, L. Peng, J. Liu and S. Song, Photo-Thermal Synergy for Boosting Photo-Fenton Activity with rGO-$ZnFe_2O_4$: Novel Photo-Activation Process and Mechanism Toward Environment Remediation, *Appl. Catal., B*, 2021, **292**, 120198.
6 Z. Xiong, Y. Wang, W. Zhu, Z. Ouyang, Y. Zhu, M. Shen, J. Xia and X. Shi, A Dual-Responsive Platform Based on Antifouling Dendrimer–CuS Nanohybrids for Enhanced Tumor Delivery and Combination Therapy, *Small Methods*, 2021, **5**, 2100204.
7 X. Liu, B. Chen, G. Wang, S. Ma, L. Cheng, W. Liu, L. Zhou and Q. Wang, Controlled Growth of Hierarchical Bi_2Se_3/CdSe-Au Nanorods with Optimized Photothermal Conversion and Demonstrations in Photothermal Therapy, *Adv. Funct. Mater.*, 2021, **31**, 2104424.
8 X. Zhen, J. Zhang, J. Huang, C. Xie, Q. Miao and K. Pu, Macrotheranostic Probe with Disease-Activated Near-Infrared Fluorescence, Photoacoustic, and Photothermal Signals for Imaging-Guided Therapy, *Angew. Chem., Int. Ed.*, 2018, **57**, 7804–7808.
9 Y. Weng, S. Guan, L. Wang, H. Lu, X. Meng, G. I. N. Waterhouse and S. Zhou, Defective Porous Carbon Polyhedra Decorated with Copper Nanoparticles for Enhanced NIR-Driven Photothermal Cancer Therapy, *Small*, 2020, **16**, 1905184.
10 M. Wu, Y. Li, N. An and J. Sun, Applied Voltage and Near-Infrared Light Enable Healing of Superhydrophobicity Loss Caused by Severe Scratches in Conductive Superhydrophobic Films, *Adv. Funct. Mater.*, 2016, **26**, 6777–6784.
11 T. Li, Y. Li, X. Wang, X. Li and J. Sun, Thermally and Near-Infrared Light-Induced Shape Memory Polymers Capable of Healing Mechanical Damage and Fatigued Shape Memory Function, *ACS Appl. Mater. Interfaces*, 2019, **11**, 9470–9477.

12 X. Jin, X. Qi, Y. Wang, J. Yang, H. Li, Z. Zhou and Y. Wang, Polypyrrole/Helical Carbon Nanotube Composite with Marvelous Photothermoelectric Performance for Longevous and Intelligent Internet of Things Application, *ACS Appl. Mater. Interfaces*, 2021, **13**, 8808–8822.

13 B. Kim, C. Cho, M. Han, A.-J. Attias and E. Kim, Giant Photo-Magneto-Thermoelectric Effect of End-On Oriented PEDOT Grown from Self-Assembled 3D Tectons, *Adv. Funct. Mater.*, 2021, 2105297.

14 B. Kim, H. Shin, T. Park, H. Lim and E. Kim, NIR-Sensitive Poly(3,4-ethylenedioxyselenophene) Derivatives for Transparent Photo-Thermo-Electric Converters, *Adv. Mater.*, 2013, **25**, 5483–5489.

15 W. Xu, H. Liu, D. Zhou, X. Chen, N. Ding, H. Song and H. Ågren, Localized Surface Plasmon Resonances in Self-Doped Copper Chalcogenide Binary Nanocrystals and Their Emerging Applications, *Nano Today*, 2020, **33**, 100892.

16 W. Xie, Y. Ren, B. Yu, X. Yang, M. Gao, J. Ma, Y. Zou, P. Xu, X. Li and Y. Deng, Self-Hybrid Transition Metal Oxide Nanosheets Synthesized by A Facile Programmable and Scalable Carbonate-Template Method, *Small*, 2021, **17**, 2103176.

17 Y. Wu, W. Xiong, Z. Wang, Y. Wang, K.-y. Sun, X. Song, Z. Lv, W. Xu, W. Zhong, X. Zou, H.-L. Cai and X. Wu, Self-Assembled MXene-Based Schottky-Junction Upon Transition Metal Oxide for Regulated Tumor Microenvironment and Enhanced CDT/PTT/MRI Activated by NIR Irradiation, *Chem. Eng. J.*, 2022, **427**, 131925.

18 M. Li, S. Fu, L. A. Lucia and Y. Wang, Ultra-Efficient Photo-Triggerable Healing and Shape-Memory Nanocomposite Materials Doped with Copper Sulfide Nanoparticles, *Compos. Sci. Technol.*, 2020, **199**, 108371.

19 Y. Ji, W. Xu, D. Li, D. Zhou, X. Chen, N. Ding, J. Li, N. Wang, X. Bai and H. Song, Semiconductor Plasmon Enhanced Monolayer Upconversion Nanoparticles for High Performance Narrowband Near-Infrared Photodetection, *Nano Energy*, 2019, **61**, 211–220.

20 S. Li, Z. Zhang, L. Yan, S. Jiang, N. Zhu, J. Li, W. Li and S. Yu, Fast Synthesis of CuS and Cu_9S_5 Microcrystal Using Subcritical and Supercritical Methanol and Their Application in Photocatalytic Degradation of Dye in Water, *J. Supercrit. Fluids*, 2017, **123**, 11–17.

21 X. Luo, H. Hu, Z. Pan, F. Pei, H. Qian, K. Miao, S. Guo, W. Wang and G. Feng, Efficient and Stable Catalysis of Hollow Cu_9S_5 Nanospheres in The Fenton-Like Degradation of Organic Dyes, *J. Hazard. Mater.*, 2020, **396**, 122735.

22 H. Niu, Y. Liu, B. Mao, N. Xin, H. Jia and W. Shi, In-Situ Embedding MOFs-Derived Copper Sulfide Polyhedrons in Carbon Nanotube Networks for Hybrid Supercapacitor with Superior Energy Density, *Electrochim. Acta*, 2020, **329**, 135130.

23 C. J. Raj, M. Rajesh, R. Manikandan, W.-g. Lee, K. H. Yu and B. C. Kim, Direct Fabrication of Two-Dimensional Copper Sulfide Nanoplates on Transparent Conducting Glass for Planar Supercapacitor, *J. Alloys Compd.*, 2018, **735**, 2378–2383.

24 M. Loloei, M. Omidkhah, A. Moghadassi and A. E. Amooghin, Preparation and Characterization of Matrimid® 5218 Based Binary and Ternary Mixed Matrix Membranes for CO_2 Separation, *Int. J. Greenhouse Gas Control*, 2015, **39**, 225–235.

25 F. Russo, R. Castro-Muñoz, F. Galiano and A. Figoli, Unprecedented Preparation of Porous Matrimid® 5218 Membranes, *J. Membr. Sci.*, 2019, **585**, 166–174.

26 J. Zhao, K. Yu, Y. Hu, S. Li, X. Tan, F. Chen and Z. Yu, Discharge Behavior of Mg–4 wt% Ga–2 wt% Hg Alloy as Anode for Seawater Activated Battery, *Electrochim. Acta*, 2011, **56**, 8224–8231.

27 F. Tao, Y. Zhang, K. Yin, S. Cao, X. Chang, Y. Lei, D. Wang, R. Fan, L. Dong, Y. Yin and X. Chen, Copper Sulfide-Based Plasmonic Photothermal Membrane for High-Efficiency Solar Vapor Generation, *ACS Appl. Mater. Interfaces*, 2018, **10**, 35154–35163.

28 W. Pei, J. Zhang, H. Tong, M. Ding, F. Shi, R. Wang, Y. Huo and H. Li, Removal and Reutilization of Metal Ions on ZIF-67/GO Membrane *via* Synergistic Photocatalytic-Photothermal Route, *Appl. Catal., B*, 2021, **282**, 119575.

29 A. Agrawal, S. H. Cho, O. Zandi, S. Ghosh, R. W. Johns and D. J. Milliron, Localized Surface Plasmon Resonance in Semiconductor Nanocrystals, *Chem. Rev.*, 2018, **118**, 3121–3207.

30 Q. Feng, Y. Xu, B. Hu, L. An, J. Lin, Q. Tian and S. Yang, A Smart Off–On Copper Sulfide Photoacoustic Imaging Agent Based on Amorphous–Crystalline Transition for Cancer Imaging, *Chem. Commun.*, 2018, **54**, 10962–10965.

31 Y. Tang, W. He, S. Wang, Z. Tao and L. Cheng, New Insight into The Size-Controlled Synthesis of Silver Nanoparticles And Its Superiority in Room Temperature Sintering, *CrystEngComm*, 2014, **16**, 4431–4440.

32 Y. Xie, A. Riedinger, M. Prato, A. Casu, A. Genovese, P. Guardia, S. Sottini, C. Sangregorio, K. Miszta, S. Ghosh, T. Pellegrino and L. Manna, Copper Sulfide Nanocrystals with Tunable Composition by Reduction of Covellite Nanocrystals with Cu^+ Ions, *J. Am. Chem. Soc.*, 2013, **135**, 17630–17637.

33 Q. W. Shu, C. M. Li, P. F. Gao, M. X. Gao and C. Z. Huang, Porous Hollow CuS Nanospheres with Prominent Peroxidase-Like Activity Prepared in Large Scale By A One-Pot Controllable Hydrothermal Step, *RSC Adv.*, 2015, **5**, 17458–17465.

34 Y. Wang, L. An, J. Lin, Q. Tian and S. Yang, A Hollow Cu_9S_8 Theranostic Nanoplatform Based on A Combination of Increased Active Sites and Photothermal Performance in Enhanced Chemodynamic Therapy, *Chem. Eng. J.*, 2020, **385**, 123925.

35 J. Zhu, X. Peng, W. Nie, Y. Wang, J. Gao, W. Wen, J. N. Selvaraj, X. Zhang and S. Wang, Hollow Copper Sulfide Nanocubes as Multifunctional Nanozymes for Colorimetric Detection of Dopamine and Electrochemical Detection of Glucose, *Biosens. Bioelectron.*, 2019, **141**, 111450.

36 Z. Chen, J. W. Chang, C. Balasanthiran, S. T. Milner and R. M. Rioux, Anisotropic Growth of Silver Nanoparticles Is Kinetically Controlled by Polyvinylpyrrolidone Binding, *J. Am. Chem. Soc.*, 2019, **141**, 4328–4337.

37 K. M. Koczkur, S. Mourdikoudis, L. Polavarapu and S. E. Skrabalak, Polyvinylpyrrolidone (PVP) in Nanoparticle Synthesis, *Dalton Trans.*, 2015, **44**, 17883–17905.
38 C. Coughlan, M. Ibáñez, O. Dobrozhan, A. Singh, A. Cabot and K. M. Ryan, Compound Copper Chalcogenide Nanocrystals, *Chem. Rev.*, 2017, **117**, 5865–6109.
39 S. Goel, F. Chen and W. Cai, Synthesis and Biomedical Applications of Copper Sulfide Nanoparticles: From Sensors to Theranostics, *Small*, 2014, **10**, 631–645.
40 M. H. Huang, S. Mao, H. Feick, H. Yan, Y. Wu, H. Kind, E. Weber, R. Russo and P. Yang, Room-Temperature Ultraviolet Nanowire Nanolasers, *Science*, 2001, **292**, 1897–1899.
41 Q. Tian, M. Tang, Y. Sun, R. Zou, Z. Chen, M. Zhu, S. Yang, J. Wang, J. Wang and J. Hu, Hydrophilic Flower-Like CuS Superstructures as an Efficient 980 nm Laser-Driven Photothermal Agent for Ablation of Cancer Cells, *Adv. Mater.*, 2011, **23**, 3542–3547.